Immunity
Article

Structures of an MHC Class I Molecule from B21 Chickens Illustrate Promiscuous Peptide Binding

Michael Koch,[1,7,16] Simon Camp,[2,7] Trevor Collen,[2,7,17] David Avila,[3,9] Jan Salomonsen,[3,10] Hans-Joachim Wallny,[3,11] Andrew van Hateren,[2] Lawrence Hunt,[2] Jansen P. Jacob,[2] Fiona Johnston,[2] Denise A. Marston,[2,12] Iain Shaw,[2,13] P. Rod Dunbar,[4,14] Vincenzo Cerundolo,[4] E. Yvonne Jones,[1,8,*] and Jim Kaufman[2,3,5,6,8,15,*]

[1]Cancer Research UK Receptor Structure Research Group, The Henry Wellcome Building for Genomic Medicine, Roosevelt Drive, Headington, Oxford OX3 7BN, UK
[2]Institute for Animal Health, Compton, Berks RG20 7NN, UK
[3]Basel Institute for Immunology, Grenzacherstrasse 487, CH-4005 Basel, Switzerland
[4]Tumour Immunology Unit, Weatherall Institute of Molecular Medicine, Oxford University, Oxford OX3 9DS, UK
[5]University of Cambridge, Department of Pathology, Tennis Court Road, Cambridge CB2 1QP, UK
[6]Department of Veterinary Medicine, Madingley Road, Cambridge CB3 0ES, UK
[7]These authors contributed equally to this work.
[8]These authors contributed equally to this work.
[9]Present address: Hoffman-La Roche, CH-4005 Basel, Switzerland.
[10]Present address: Copenhagen University, DK-1870 Frederiksberg C, Denmark.
[11]Present address: Novartis Pharma AG, CH-4002 Basel, Switzerland.
[12]Present address: Veterinary Laboratories Agency, New Haw, Addlestone, Surrey KT15 3NB, UK.
[13]Present address: National Diagnostics Centre, National University of Ireland, Galway, Ireland.
[14]Present address: University of Auckland, Auckland 1142, New Zealand.
[15]Present address: University of Cambridge, Department of Pathology, Tennis Court Road, Cambridge CB2 1QP, UK.
[16]Present address: Centre Européen de Biologie et de Génomique Structurales, Parc d'Innovation, 1 rue Laurent Fries, F-67404 Illkirch Cedex, France.
[17]We dedicate this paper to Trevor Collen, who died during the course of the project—a tragic loss many years too soon.
*Correspondence: yvonne@strubi.ox.ac.uk (E.Y.J.), jfk31@cam.ac.uk (J.K.)
DOI 10.1016/j.immuni.2007.11.007

SUMMARY

Little is known about the structure of major histocompatibility complex (MHC) molecules outside of mammals. Only one class I molecule in the chicken MHC is highly expressed, leading to strong genetic associations with infectious pathogens. Here, we report two structures of the MHC class I molecule BF2*2101 from the B21 haplotype, which is known to confer resistance to Marek's disease caused by an oncogenic herpesvirus. The binding groove has an unusually large central cavity, which confers substantial conformational flexibility to the crucial residue Arg9, allowing remodeling of key peptide-binding sites. The coupled variation of anchor residues from the peptide, utilizing a charge-transfer system unprecedented in MHC molecules, allows peptides with conspicuously different sequences to be bound. This promiscuous binding extends our understanding of ways in which MHC class I molecules can present peptides to the immune system and might explain the resistance of the B21 haplotype to Marek's disease.

INTRODUCTION

Classical class I molecules encoded in the major histocompatibility complex (MHC) are crucial to protection from numerous pathogens, and the genes for such molecules have been identified in many jawed vertebrates, down to bony and cartilaginous fish (Flajnik and Kasahara, 2001; Kelley et al., 2005). However, beyond the gene sequences, little is known about the structure and function of MHC class I molecules outside of mammals.

Among the nonmammalian vertebrates, the chicken is the best characterized in terms of the immune response, the genetics of disease resistance and vaccine response, and the genomic structure and function of the MHC. Chickens are assailed by a large variety of pathogens, including important zoonotic organisms such as avian influenza H5N1. Among the potential immune response loci, the chicken MHC can determine striking resistance and susceptibility to infectious pathogens, as well as response to vaccines (Bacon, 1987; Bacon et al., 1987; Plachy et al., 1992). The first such association to be described, and still among the strongest known, is the association of the MHC haplotype B21 with resistance to Marek's disease, caused by an alphaherpesvirus (Hutt and Cole, 1947; Hansen et al., 1967; Briles et al., 1977).

Compared to the MHC of typical mammals, the chicken MHC is much smaller and simpler, with a different

genomic organization (Guillemot et al., 1988; Kaufman et al., 1995; Kaufman et al., 1999a). Recombination is rare within the chicken MHC, and this property has been proposed to allow coevolution between interacting genes, such as the class I, TAP1, TAP2, and tapasin genes. A consequence of this coevolution is the expression of a single dominantly expressed class I molecule, explaining the striking associations with resistance to certain infectious pathogens (Kaufman et al., 1995; Kaufman et al., 1999a, 1999b; Wallny et al., 2006). Indeed, the features of genomic organization leading to the high expression of a single class I molecule are found in many if not most nonmammalian vertebrates (Kaufman, 1999).

The structural basis for peptide binding to mammalian MHC class I molecules is now fairly well understood (Stern and Wiley, 1994; Wilson and Fremont, 1993; Madden, 1995; Matsumura et al., 1992). In general, the peptides bound to classical MHC class I molecules have N and C termini that interact with invariant MHC class I residues in pockets A and F at either end of the peptide-binding groove. The peptides are usually octamers or nonamers that make invariant and polymorphic contacts all along the groove, although longer peptides that bulge out in the middle of the groove are described. Comparisons of structures show that the main-chain conformation of the bound peptide is usually conserved over the N- and C-terminal portions but can show substantial differences in the central portion (even between peptides of similar length, e.g., nonamers).

In mammals, the peptide-binding motif for a particular MHC classical class I molecule generally specifies two or more positions (anchor positions) at which all suitable peptides have one or a very limited set of residues (Rammensee, 1995; Rammensee et al., 1995). Structural analyses have revealed that the side chains of these anchor residues (along with secondary anchors) interact with polymorphic residues that define the binding specificities of a series of pockets (B through F) along the peptide-binding groove. Anchor residues are found usually at peptide position 2 (P_2) interacting with pocket B, sometimes at position 5 or 6 (P_5 or P_6) interacting with pocket C or E, and usually at the C-terminal residue (P_C) binding in pocket F (Madden, 1995). High-resolution crystal structures have demonstrated that tightly bound water molecules are frequently vital in the optimization of the hydrogen bonding and shape complementarity of the peptide-binding groove interface, e.g., HLA-B53 (Smith et al., 1996).

Only in the chicken, among all nonmammalian vertebrates, are there sequences of individual peptides and peptide pools leading to peptide motifs for the dominantly expressed classical MHC class I molecule. For some MHC haplotypes, such as B4, B12, and B15, it was trivial to define simple peptide motifs for octamer and nonamer peptides on the basis of sequences of peptide pools and individual peptides eluted from MHC class I molecules. Moreover, the location and chemical nature of the polymorphic residues in the groove of the corresponding MHC class I molecules made it easy to rationalize the specificity of binding (Kaufman et al., 1995; Wallny et al., 2006).

In contrast, it was very difficult to discern a clear MHC class I peptide motif for some chicken MHC haplotypes, such as B21. Here, we report first the sequences of peptide pools from cells of the B21 haplotype. We then determined the structure of the dominantly expressed MHC class I molecule of the B21 haplotype, the BF2*2101 molecule, bound to two peptides with conspicuously different sequences. Finally, we used substituted peptides to define a preliminary peptide motif and used the motif to illustrate how the BF2*2101 molecule could explain the resistance to Marek's disease. The results provide the first structures of MHC molecules outside of mammals, point to a striking mode of binding that explains the initially confusing data for the peptides, and extend our understanding of the ways in which MHC class I molecules can present peptides to the immune system.

RESULTS

Sequences of Peptide Pools Fail to Indicate a Clear Motif for B21 Class I Molecules

Compared to other chicken MHC haplotypes (Wallny et al., 2006), far fewer peptides were isolated from cells of the B21 haplotype, as illustrated by reverse-phase high-pressure liquid chromatography (HPLC) chromatograms of peptides isolated from equivalent numbers of blood cells from B15 and B21 chickens (Figures 1A and 1B). Unlike the pool sequence from B15, for which the anchor residues are clear (Arg at P_2, and mainly Tyr at P_8 and P_9), there were no obvious anchor residues for B21. At every peptide position, including P_2, multiple amino acids of very different sizes and chemical natures were present (Figures 1C and 1D). Overall, 12 independent preparations of MHC class I molecules were isolated by affinity chromatography (from blood leukocytes, erythrocytes, and spleen cells, from four different lines of chicken bearing the B21 haplotype, and with two different monoclonal antibodies for isolation), and in no case did the sequence of the total pool of peptides give an obvious, consistent, and simple peptide motif (Figure S1 available online). Relatively few individual peptides were isolated, even with very large scale preparations, and both the lengths and sequences of these peptides varied widely (data not shown).

Among the peptides isolated from several different preparations were an 11-mer (GHAEEYGAETL) and a 10-mer (REVDEQLLSV), which have strikingly dissimilar sequences. A soluble heavy chain for BF2*2101 (the dominantly expressed MHC class I of the B21 haplotype) and β_2-microglobulin (β_2m) were expressed in bacteria, isolated from inclusion bodies in denaturing buffers, and used to show that the same B21 class I molecule assembled upon renaturation with either of the two dissimilar peptides (Figure S2). Thus, a single class I molecule can be responsible for the complex peptide motif of the B21 haplotype.

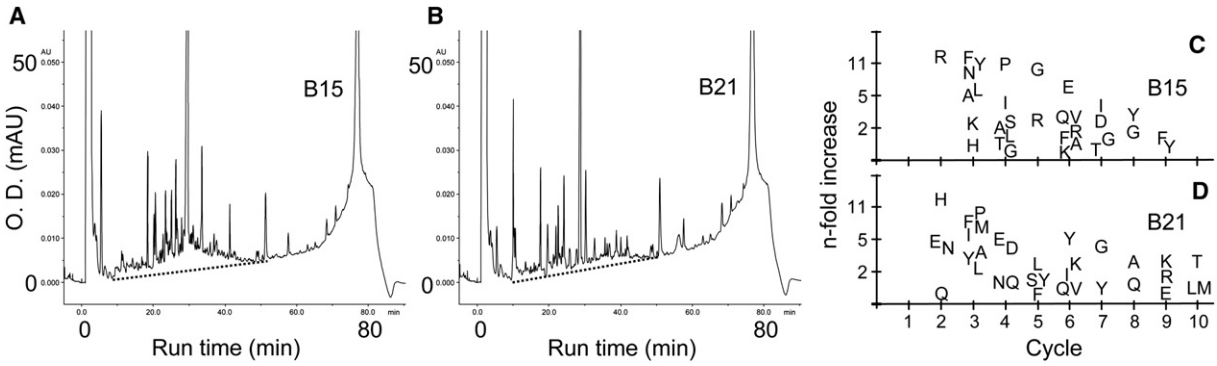

Figure 1. In Comparison to B15, Fewer Peptides and No Clear Motif Was Found for Class I Molecules from the B21 Haplotype

MHC class I molecules from equal numbers of H.B15 and H.B21A blood cells were isolated by affinity chromatography.

(A and B) Peptides were eluted and separated by HPLC (O.D., optical density at 210 nm; mAU, milli absorbance units), with the quantity of peptides indicated by the area above the dotted baseline.

(C and D) Pools of peptides were analyzed by Edman degradation, with the graphs showing the n-fold increase of a particular amino acid derivative at each cycle of degradation over the previous cycle (based on pmol at each cycle; letters indicate amino acid derivatives with the single letter code) versus cycle number.

The Overall Structure of BF2*2101 Shows a Large Rotation of the α3 Domain Compared to Mammals

Crystals of BF2*2101-11-mer and BF2*2101-10-mer grew in the space groups $P2_12_12_1$ with one molecule per crystallographic asymmetric unit and in $P2_1$ with two molecules in the asymmetric unit, respectively. We determined the structure of BF2*2101-11-mer by molecular replacement [with human MHC class I molecule HLA-B27 (Hulsmeyer et al., 2004) as search model] and refined it to 2.1 Å resolution (Table 1). The BF2*2101-10-mer structure was phased with the BF2*2101-11-mer structure and refined to 2.6 Å resolution (Table 1). The two copies of BF2*2101-11-mer and the one of BF2*2101-10-mer have nearly identical main-chain structures.

These BF2*2101 structures show the same overall domain arrangement and topology as that previously reported for mammalian MHC class I structures. The α1 and α2 domains, which together form the peptide-binding groove from two α helices atop an eight-stranded β sheet, rest mostly on the noncovalently associated light chain β_2m, with the α3 domain beneath (Figures 2A and 2B). Although the root-mean-square difference (rmsd) between Cα positions of chicken and mammals for each domain are low, ranging from 0.8 to 1.5 Å (Table S1), there are some differences in detail (Figures 2C and 2D). Four interstrand loops of the binding groove β sheet are different (Figure 2D), affected by sequence differences and deletions. These sequence characteristics are conserved in all chicken MHC class I molecules (and include an N linked glycosylation site in the α1 domain β3-β4 loop). The N- and C-terminal portions of the α2 helix (Figure 2D) and the α3 domain β1-β2 loop (Figure S3) are also moved slightly compared to those of mammals.

However, there are large differences in the relative positions of the domains. The α3 domain in the BF2*2101 structures is rotated by 14°–29° from its position in mammalian structures (Figure 2C, Figure S3 and Table S1). The position of the α3 domain is known to be flexible in mammals (Madden, 1995), but the three copies of the BF2*2101 structure (ranging over 6°) are positioned far beyond the mammalian molecules. The α3 domain orientation is in part complemented by changes of 3°–9° in the position of chicken β_2m compared to mammalian β_2m (Figure 2C, Figure S3). These domain reorientations mean that different parts of the α3 and β_2m domain surfaces interface in BF2*2101 compared to mammalian structures (Table S2); however, the total buried surface area remains similar [3500 $Å^2$ and 3000 $Å^2$ for BF2*2101 and HLA-A2 (Khan et al., 2000), respectively].

The α3 domain is the major site of interaction with CD8 in mammals. The structure of BF2*2101 confirms predictions (Kaufman et al., 1992) that the surface of the α3 domain is diverged from mammals, with only two protuberant residues conserved, Glnα222(226) and Aspα223(227) (numbers in parentheses from human sequence; numbers without parentheses from chicken sequence or common to both) (Figure 2C). Of the residues predicted to be involved in CD8 binding, on the basis of the structures of human and mouse CD8-MHC class I complexes (Gao et al., 1997; Kern et al., 1998), most are not conserved in chicken (Table S3). However, Glnα222(226) and Aspα223(227) make multiple interactions with three conserved CD8α residues [Ser(35)34, Tyr(50)51, and Ser(52)53], suggesting that the core features of this fundamental interaction are conserved.

The Binding Groove of BF2*2101 Has a Large Central Cavity, Allowing Argα9 Great Flexibility

The various binding groove pockets originally defined for mammalian MHC class I molecules (Saper et al., 1991) are present in BF2*2101. However, in BF2*2101 several of these pockets have characteristics that are unique (Figure 3).

Of the residues in contact with the peptide N and C termini, in pockets A and F, respectively, only the pocket F residue Argα83 is not identical with mammals

Table 1. Statistics for Data Collection and Refinement

Crystallographic Statistics	BF2*2101-11-mer	BF2*2101-10-mer
Data Collection		
Resolution range (Å)[a]	20–2.10 (2.17–2.10)	30–2.60 (2.69–2.60)
Number of collected reflections	156,087	104,981
Unique reflections	22,643	30,205
Completeness (%)	100 (100)	97.9 (90.0)
R_{merge} (%)[b]	14.3 (65.0)	9.7 (32.3)
I/σI	17.1 (3.6)	13.2 (2.8)
Space group	$P2_12_12_1$	$P12_11$
Unit cell: Dimensions (Å) (a, b, c)	71.3, 72.2, 72.7	57.8, 89.1, 100.6
Unit cell: Angles (°) (α, β, γ)	90, 90, 90	90, 99.9, 90
Source	ESRF BM14	ESRF BM14
Model Refinement		
Resolution range (Å)	20–2.10	20–2.60
Number of reflections (test set)[c]	21,364 (1,135)	28,626 (1,511)
R_{cryst} (%)[d]	23.0	22.7
R_{free} (%)[e]	28.6	28.8
Number of nonhydrogen protein atoms	2,983	5,931
Number of water molecules	193	128
Number of nonhydrogen ligand atoms	83	166
Average B factors: Protein (Å^2)	26.2	34.8
Average B factors: Water (Å^2)	28.4	23.6
Average B factors: Peptide (Å^2)	20.2	39.7
r.m.s deviation from ideality: Bond lengths (Å)	0.012	0.011
r.m.s deviation from ideality: Bond angles (°)	2.33	1.34
r.m.s deviation B factors (bonded atoms): Main Chain (Å^2)	2.26	0.75
Ramachandran plot: Favored (%)	92.5	89.7
Ramachandran plot: Allowed (%)	6.5	9.0
Ramachandran plot: Generous (%)	0.6	0.5
Ramachandran plot: Unfavored (%)	0.3	0.8

[a] Values in parentheses refer to the highest resolution shell of data.
[b] $R_{merge} = \Sigma h \Sigma i \mid I_i(hkl) - < I(hkl) > I / \Sigma h \Sigma i I_i(hkl)$, where $I_i(hkl)$ is the 'ith' measurement of reflection hkl and < I(hkl) > is the weighted mean of all measurements of reflection hkl.
[c] Test set is a randomly chosen set of reflections omitted from the refinement process.
[d] $R_{cryst} = \Sigma h \mid\mid F_{obs}(hkl)| - | F_{calc}(hkl)|| / \Sigma h |F_{obs}(hkl)|$, where F_{obs} and F_{calc} are the observed and calculated structure factor alplitudes, respectively.
[e] R_{free} is equivalent to R_{cryst} but calculated for the test set of reflections.

[Tyrα(84)] but is identical with classical MHC class I molecules from all nonmammalian vertebrates (Kaufman et al., 1994). The portion of pocket F that accommodates the anchor residue side chain for the C-terminal residue P_C is lined with primarily hydrophobic residues (Figure 3A, Table S4), very similar to many mammalian MHC class I molecules.

Pocket B (accommodating anchor residues at peptide position P_2; Figure 3B, Table S4) is polar in BF2*2101 as a result of charged residues Aspα24 and Gluα62(63). Most residues contributing to this pocket are equivalent in BF2*2101 and mammalian MHC class I molecules. However, Alaα43(45) (which is highly polymorphic in mammals and an important P_2 contact for many, but not all, mammalian MHC class I molecules) is blocked from contributing to the BF2*2101 B pocket by Metα34. The most distinctive property of the pocket results from the unusual conformational flexibility of the Argα9 side chain.

Pocket D opens into a large cavity that includes pockets C and E, comprising the entire central section of the binding groove (Figures 3C and 3D, Table S4). The relatively small side chains of Serα69(70) (pointing into the binding groove from the α1 helix) and Serα97(99) (pointing upward from the β1 strand of the α2 domain) contribute to the spaciousness of this central region. The equivalent residues in mammals generally have bulky side chains [His/Lysα(70) and Tyr/Pheα(99)], which separate the B, C, and D pockets. In BF2*2101 the C, D, and E pockets are not identifiable as distinct pockets, but we use the mammalian nomenclature to refer to these regions of the overall cavity. It is the open nature of the central cavity in BF2*2101 that allows conformational flexibility for the side chain of Argα9 (Figure 3C, Table S4).

The N- and C-Terminal Peptide Conformations Are Similar to Mammals but with Three Anchor Residues

Both the 11-mer and 10-mer peptides are anchored in the BF2*2101 binding groove by polar residues at P_2, bulge out of the binding groove in the central portion, and then dip distinctively into the C-terminal region anchored by the P_{C-2} residue as well as a hydrophobic P_C residue (Figures 4A and 4B). For both peptides, the N and C termini occupy essentially identical positions. Peptide side chains point into the binding groove at P_2, P_3, P_{C-3}, P_{C-2}, and P_C, whereas those at the P_1, P_4, P_5, P_6, (P_7 for the 11-mer), and P_{C-1} positions are surface exposed (Figures 4C and 4D). The main-chain conformations of the N-terminal portion (P_1 through P_3) and the C-terminal portion (P_{C-1} and P_C) are similar to those observed for peptides bound by mammalian MHC class I molecules (although the P_{C-1} residue is positioned deeper within the binding groove in BF2*2101; see below).

The hydrogen bond networks that tether the peptide N and C termini (Figures 4C and 4D) are highly conserved between BF2*2101 and mammalian molecules. For pocket A, all the participants in the hydrogen bonding network, including Tyrα7(7), Tyrα58(59), Gluα62(63), Tyrα156(159), Tyrα168(171), plus an ordered water molecule are conserved. In pocket F, the hydrogen bonds between MHC class I residues Thrα140(143), Lysα143(146), and the peptide C terminus are strictly conserved, whereas the interactions of Argα83 substitute for those made by Tyrα(84) in mammals. Consequently, the positions of the peptide N and C termini are essentially equivalent between chicken and mammalian structures (<1 Å difference), except that in BF2*2101, the distance between the Trpα144(147) side chain and the P_{C-1} carbonyl oxygen is too great to form the hydrogen bond found in mammals.

As in other classical MHC class I structures, the side chain of the P_1 residue points out of the peptide-binding groove. However, in the BF2*2101-10-mer structure, the side chains of the Arg residues at P_1 and α61(62) make a distinctive stacking interaction between their guanidinium groups. A similar phenomenon has been noted in a human HLA-B27 peptide complex (Hulsmeyer et al., 2004).

The P_2 residue is an anchor as in many mammalian structures, with the side chain inserting into pocket B and the main-chain nitrogen making a hydrogen bond to the Gluα62(63) side chain. In the 11-mer structure, Gluα62(63) also hydrogen bonds to the P_2 side chain (Figure 3B). A second charged residue, Aspα24, interacts with the P_2 side chain in both BF2*2101 10-mer and 11-mer structures, understandably for the His2 in the 11-mer (because it is electrostatically favorable; Figure 4A) but unexpectedly for the Glu2 in the 10-mer (because it involves two acidic residues; Figure 4B). The mechanism by which this apparent charge clash is neutralized involves Argα9 (see below).

As in mammals, the P_3 residue (11-mer Ala3, 10-mer Val3) occupies the D pocket (which opens into the central cavity as described above), stacking against the side chain of Tyrα156(159). After P_3, the peptide in both structures rears out of the groove. The main chain descends back into the binding groove at the P_{C-3} residue (11-mer Ala8, 10-mer Leu7), the side chain of which interacts with the central cavity residues Trpα144(147) and Tyrα149(156) at pocket E.

In both structures, the P_{C-2} residue (11-mer Glu9, 10-mer Leu8) is an anchor deeply buried in the region of the central cavity corresponding to pocket C (Figures 4C and 4D). The side chains of the P_{C-2} residues point back toward the N terminus of the peptide, and their interactions are critical for the specificity of binding (see below).

As in mammals, the P_{C-1} residue (11-mer Thr10, 10-mer Ser9) points out of the groove and the P_C residue (11-mer Leu11, 10-mer Val10) is an anchor occupying the F pocket (Figures 4C and 4D). The P_C side chains form favorable interactions with the hydrophobic residues that line the pocket, but neither P_C side chain fills the available space (Figure 3A, Table S4). This suggests that large aromatic P_C residues can be accommodated in pocket F. In agreement, peptides with hydrophobic P_C residues including Val, Ile, Leu, Met, Phe, and Trp can assemble into stable complexes with BF2*2101 (data not shown).

The Center of the Peptide Bulges Out with Many Contiguous Residues Exposed

The 11-mer and 10-mer peptides both have central regions that bulge out of the binding groove, but their conformations are very different. The greatest divergence occurs immediately after P_3, so that at P_4 the 10-mer and 11-mer residues are no longer in register (Figure 4E). The more bulged conformation of the 11-mer accommodates two residues (Glu4 and Glu5) before returning into register with the 10-mer peptide at the P_{C-5} residue (11-mer Tyr6, 10-mer Glu5). For the 11-mer, the bigger bulge, plus the relatively small side-chains of the P_3 and P_{C-3} residues (both Ala), results in a large cavity of some 150 $Å^3$ formed between the peptide and the central section of the groove (Figure 4C). The cavity accommodates eight tightly bound water molecules forming a well-ordered hydrogen-bonded network (Figures 4A, 4C, and 4E). In contrast, the 10-mer lies deeper within the binding groove, and this, combined with more bulky residues at P_3 and P_{C-3} (Val and Leu), results in a cavity of only 20 $Å^3$ (Figures 4B, 4D, and 4E). This space is at the limit of the volume required for the binding of a single water molecule, but composite OMIT maps provide only weak evidence for the site's being occupied. Several structures of mammalian MHC class I molecules presenting long peptides with bulged conformations have been reported (Probst-Kepper et al., 2004; Kjer-Nielsen et al., 2003; Speir et al., 2001) with water molecules also filling the space between the bulged peptide and the binding groove. However, the BF2*2101-11-mer structure is unusual in that the eight molecules forming the water cushion are completely sequestered from interaction with bulk solvent.

Both peptides expose a set of hydrophilic residues for potential interactions with T cell receptors (TCRs). In mammalian structures, residues that are prominently exposed

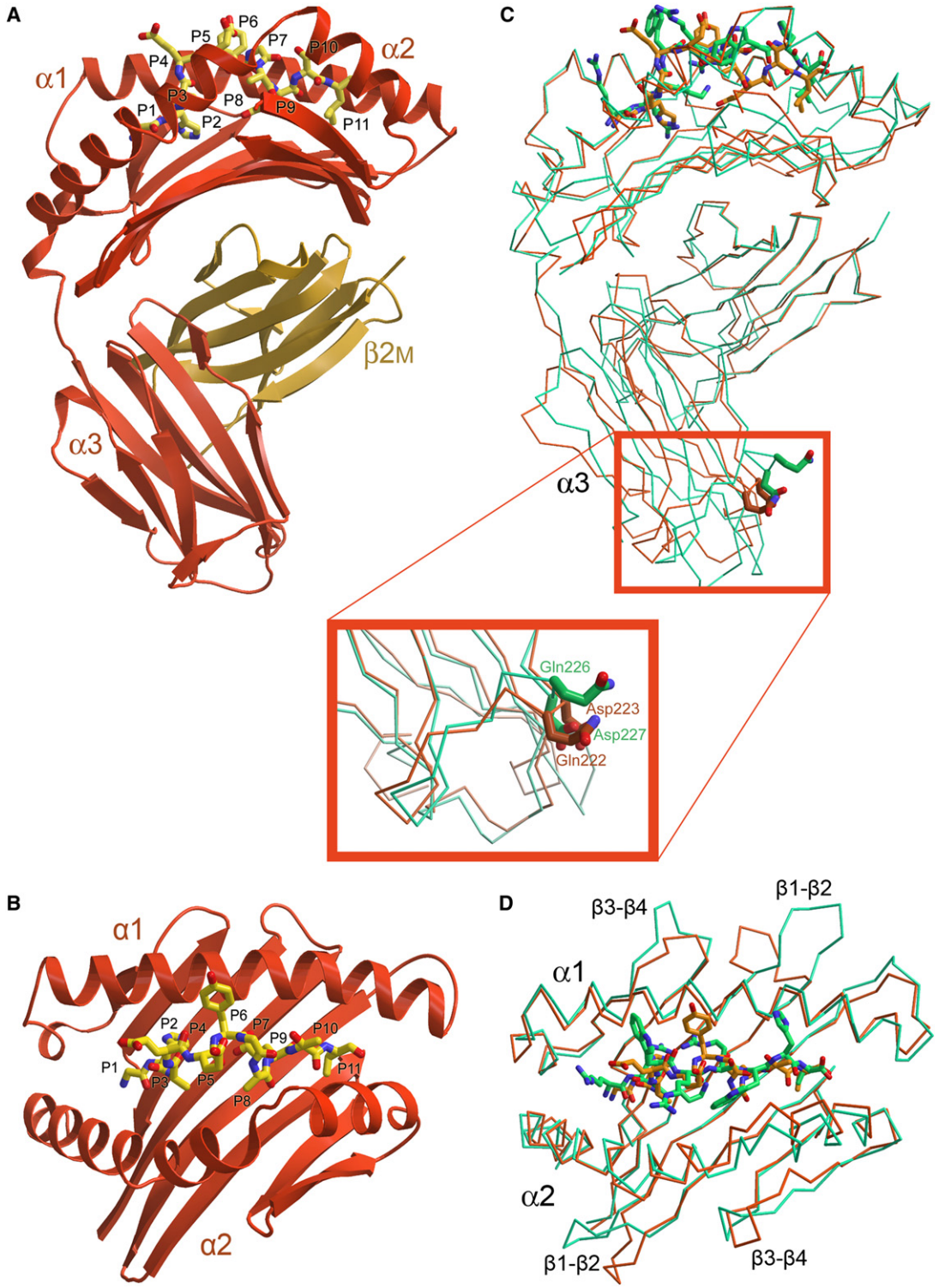

Figure 2. The Structure of the Chicken MHC Class I Molecule BF2*2101

(A and B) The heavy chain of the chicken BF2*2101 structure is shown schematically in orange and the β_2m molecule in yellow, with the 11-mer peptide represented as ball and stick. The view is sideways into (A) and from above (B) the binding groove.

(C and D) Superimposed Cα-traces of the chicken BF2*2101 molecule (orange) and human HLA-B27 (PDB entry 1OGT, green) are shown with the peptides (11-mer and HLA-B27 peptide as yellow and green carbon atoms, respectively) as ball and stick. In (C), the view is sideways into the binding groove. The superposition is based on the α1 and α2 domain and therefore highlights the shift in the orientation of the α3 domain in chicken compared to human structures. The red boxed area includes the β3-β4 loop of the α3 domain with side chains of the two residues central to CD8 binding for the

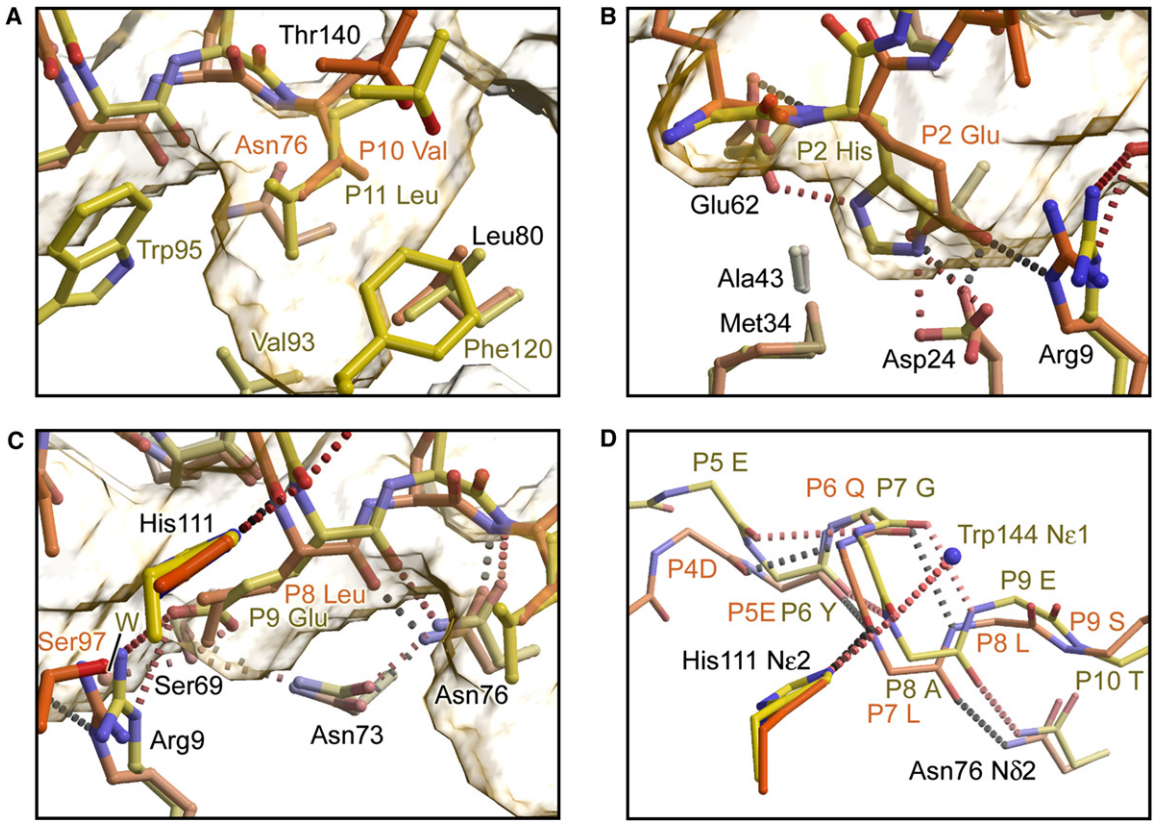

Figure 3. The Pockets of the BF2*2101 Peptide-Binding Groove

Portions of the 11-mer and 10-mer peptides (yellow and orange carbon atoms, respectively) plus the side chains of residues lining the pockets are shown as ball-and-stick models; where residues have identical conformations in the 10-mer and 11-mer structures, only the 11-mer structure is shown. The BF2*2101-11-mer binding groove is represented as a semitransparent surface. Peptide residues are labeled separately for the 11-mer (brown) and 10-mer (red), whereas heavy-chain residues are labeled in black when relating to both structures but separately when relating to the 11-mer (yellow) or the 10-mer (red) only. Hydrogen bonds are depicted as dashed lines, in red for the 11-mer and in dark red for the 10-mer.

(A) F pocket. For clarity, Val121 is not shown because it is positioned in front of the P_C side chain.

(B) B pocket.

(C) C pocket region of the central cavity.

(D) Helical turn. BF2*2101 residue side chains (for clarity in Trpα144 reduced to just the Nε1 atom) involved in three (two) intermolecular hydrogen bonds to the main chain of the 11-mer (10-mer), plus three intrapeptide hydrogen bonds, are shown as in previous panels.

at the apex of bulged peptides provide a particular focus for TCR binding [HLA-B35-13-mer-TCR complex (Tynan et al., 2005)]. For the BF2*2101-11-mer, residues Glu4, Glu5, Tyr6, and Gly7 in the bulged central region of the peptide are well exposed to solvent, as is residue Thr10 proximal to the peptide C terminus. In the BF2*2101-10-mer, the exposed peptide side chains are Arg1 at the N terminus, Asp4, Glu5, and Gln6 in the central region of the peptide (which are the most prominent), and the C-terminal proximal residue Ser9.

The peptides share similar helical turn conformations (11-mer P_7 to P_{10}, 10-mer P_6 to P_9: Figure 3D, Table S4), their main chains dipping back in toward the BF2*2101 binding groove from P_{C-4} (11-mer Gly7, 10-mer Gln6) (Figures 4C, 4D, and 4E). This distinctive peptide main-chain conformation is stabilized by three intrachain hydrogen bonds plus hydrogen bonds with the side chains of BF2*2101 residues Asnα76(77), Hisα111(114), and Trpα144(147) (the latter residue only contributing in the 11-mer structure; Figure 3D). Assembly experiments show that, unlike MHC class I molecules from the B4, B12, and B15 haplotypes, BF2*2101 will not bind octamers (data not shown). Because octamer peptides must adopt an extended main-chain conformation to

human system (PDB entry 1AKJ) shown in stick representation with green carbons and the equivalent residues in chicken shown with orange carbons. The close-up view of the red boxed area in (C) shows the superposition of BF2*2101 and HLA-B27 based on α3 domains. In (D), the view is from above the binding groove. Those α1 and α2 domain loops that show conformational differences between BF2*2101 and HLA-B27 are indicated: β1-β2 and β3-β4 loops of the α1 domain and β1-β2 and β3-β4 loops of the α2 domain. The main-chain conformations of all of the interstrand loops are well defined in the BF2*2101 structures (crystallographic B factors < 35 Å^2 and 46 Å^2 for noncharged residues and 57 Å^2 and 50 Å^2 for charged residues in the 11-mer and 10-mer, respectively).

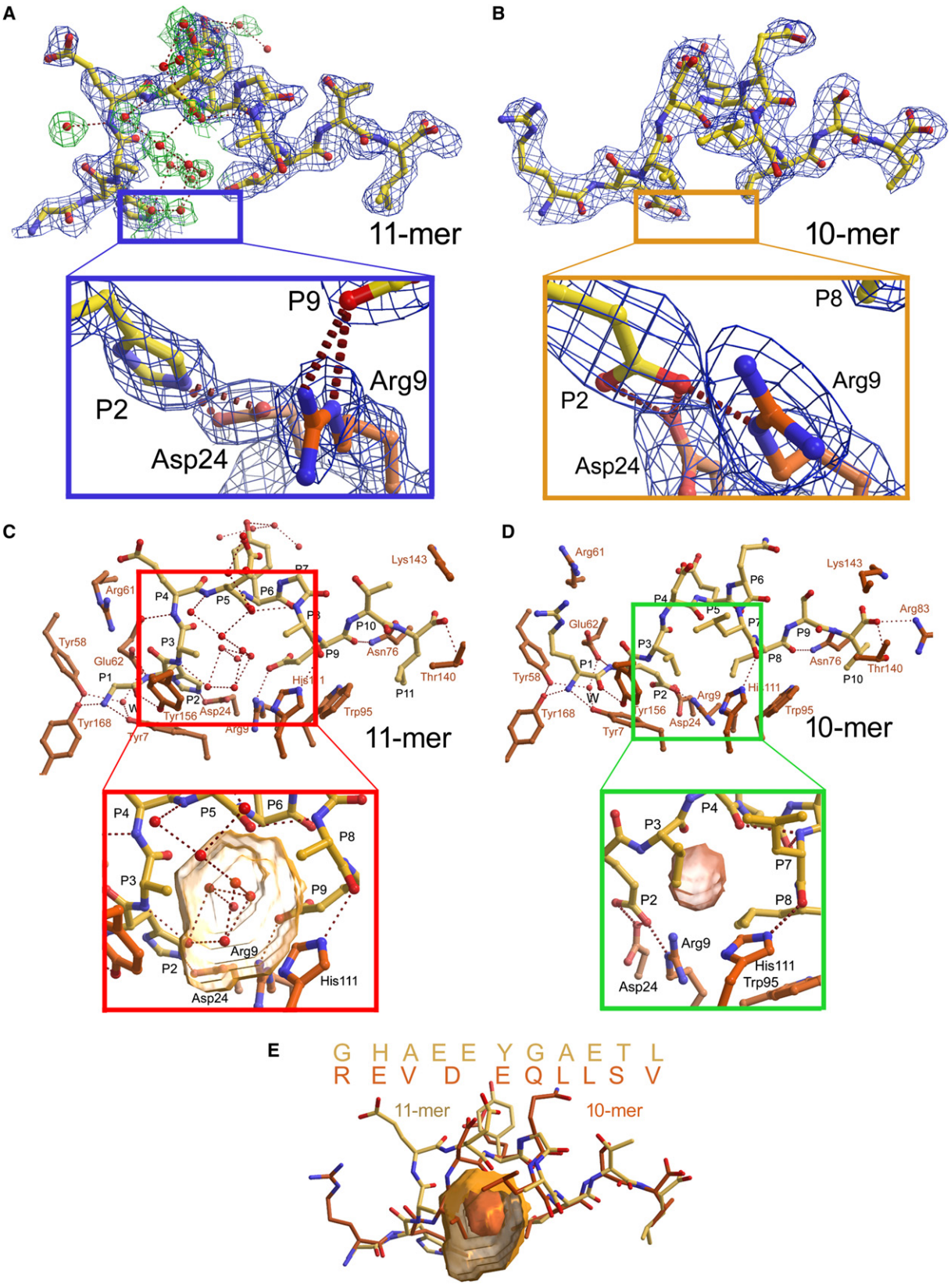
A
11-mer
P9
Arg9
P2
Asp24
B
10-mer
P8
Arg9
P2
Asp24
C
11-mer
Lys143
Arg61
Tyr58
Glu62
Asn76
Thr140
Tyr168
Tyr156
Asp24
Trp95
Tyr7
Arg9
His111
D
10-mer
Arg61
Lys143
Arg83
Glu62
Tyr58
Asn76
Thr140
Tyr168
Tyr156
Asp24
Arg9
Trp95
Tyr7
E
G H A E E Y G A E T L
R E V D E Q L L S V
11-mer
10-mer

span between pockets A and F in mammalian MHC class I molecules (Fremont et al., 1992; Reid et al., 1996; Rudolph et al., 2001), this result suggests that the helical turn conformation might be characteristic of BF2*2101 bound peptides.

The Anchor Residues P_2 and P_{C-2} Do Not Bind Independently, Allowing a Novel Peptide-Binding Strategy

Although the P_2 residue is an anchor inserted in pocket B in both BF2*2101 structures, the pool sequences show a broad range of polar and charged resides at this position (Figure 1, Figures S1 and S2). In the 11-mer, the side chain of His2 makes an electrostatically favorable interaction with the side chain of the pocket B residue Aspα24 (Figure 4A). For the 10-mer, there is also a close juxtaposition of the Glu2 and Aspα24 side chains, an apparent electrostatic clash between two negatively charged residues (distances between Aspα24 Oδ1 and P_2 Glu Oε1 and Oε2 are 2.7 and 3.0 Å, respectively; Figure 4B). Crucially, comparison of the two structures reveals a mechanism by which the hydrogen-bonding potential of this portion of the binding groove can be modulated by changes in the side-chain conformation of Argα9.

In the BF2*2101-11-mer structure, Argα9 interacts with the negatively charged Glu9, leaving Aspα24 free to interact with His2 (Figures 4A and 4C). In the BF2*2101-10-mer structure, Argα9 swivels away from the hydrophobic Leu8 to hydrogen bond to the Glu2 (2.3 Å between P2 Glu Oε2 and Arg9 Nε) (Figures 4B and 4D). In silico calculations (Li et al., 2005) indicate that the Glu2 Oε1 is protonated (Table S4) and that the three-residue network, Aspα24-Glu2-Argα9, forms a charge-relay system with no resultant net charge. Moreover, the reorientation of Argα9 leaves a suitably hydrophobic environment in pocket E for Leu8 (Figure 4D). Thus, conformational flexibility of the Argα9 side chain allows an optional contribution to the hydrogen bonding and electrostatics of both the B and E pockets. Taken together, the two structures suggest that peptide binding to the BF2*2101 molecule requires particular combinations of amino acids at position P_2 and P_{C-2}.

The Binding Groove and Peptide Conformations of BF2*2101 Are Unique

Our structural analyses reveal that the BF2*2101 binding groove has an unusually large central cavity, the result of small residues at α69(70) and α97(99). Comparisons with mammalian structures show that this distinctive open groove architecture has striking consequences for peptide binding. First, the use of the C pocket by a P_{C-2} anchor, seen in both BF2*2101 structures, is rare (Figure 5A). Out of nearly 200 structures deposited in the Protein Data Bank (PDB) (http://www.rcsb.org/pdb/home/home.do), only 12 structures of six MHC class I molecules orientate the P_{C-2} side chain into the binding groove (Figures 5B–5I). Of these mammalian structures, only one HLA-B53-nonamer complex orientates the side chain back along the binding groove, similar to the BF2*2101 structures (Figure 5E); a second nonamer peptide complexed to HLA-B53 does not have the same conformation (Smith et al., 1996). Notably, for the BF2*2101 structures, the P_{C-2} and P_{C-1} Cα atoms are positioned as much as 2.3 Å and 1.8 Å, respectively, deeper in the binding groove than they are for any mammalian structure (Figure 5A). Thus, although the tips of long P_{C-2} side chains reach to the bottom of the binding groove in several mammalian structures, the BF2*2101 structures are the only ones for which the entire P_{C-2} residue is positioned deep within the binding groove. This position is only possible because of the spacious nature of the BF2*2101 binding groove, with the P_{C-2} main chain being locked into its unique position (and requisite helical turn conformation) by hydrogen bonds to Asnα76(77) and Hisα111(114) (Figure 3D).

The second distinctive feature resulting from the open nature of the BF2*2101 binding groove is the conformational plasticity of Argα9 and the consequent coupled variation of the P_2 and P_{C-2} anchor residues. Switches in side-chain conformation have been reported previously to be one mechanism by which an MHC class I binding groove can adapt to bind different peptides (Smith et al., 1996; Fremont et al., 1992; Madden et al., 1993), but none involve residue α9. Some interplay in the P_2 and P_5 anchor residues accommodated in the B and C pockets has been noted for structures of H-2K^b (Fremont et al., 1995), a mouse MHC classical class I molecule that, like BF2*2101, has a small serine residue at position α97(99). However, in H-2K^b, Valα9 provides little potential for conformational plasticity and the effects of different anchor residue pairings are balanced by changes in bound water structure. In BF2*2101, the combination of open binding groove, side-chain flexibility at α9, and counterbalancing

Figure 4. Peptides Bound to BF2*2101

(A and B) The electron density of the 11-mer and 10-mer peptides are shown as composite OMIT maps contoured at 1.0 σ in blue for the peptide and in green for peptide-bound water molecules (both within and outside the binding groove). The blue box shows the details of the electrostatic interactions at pocket B in the BF2*2101 11-mer, and the yellow box shows the details of the three-residue Aspα24-P_2Glu-Argα9 charge-relay system at pocket B in the BF2*2101 10-mer.

(C and D) The structure of the 11-mer and 10-mer peptides (yellow carbon atoms) are shown with relevant parts of interacting residues from the binding groove (orange carbon atoms) and bound water molecules (red spheres) buried within the binding groove, one of which being the conserved water interacting with the N-terminus (W). Hydrogen bonds are depicted as dotted red lines. The red box shows a close-up view of the "water cushion" filling the central region of the binding groove in the BF2*2101-11-mer structure with the cavity (yellow surface) calculated in the absence of bound waters. The green box shows a close-up view of the central portion of the 10-mer including the small cavity present beneath the bulge region.

(E) Superposition of the sequences (single letter code) as well as of the structures of the two chicken peptides 11-mer (yellow) and 10-mer (orange) are shown, with the latter including the cavities depicted in the red and green boxes. Note the two peptides run out of register at P_3 and return to register at P_{C-5}.

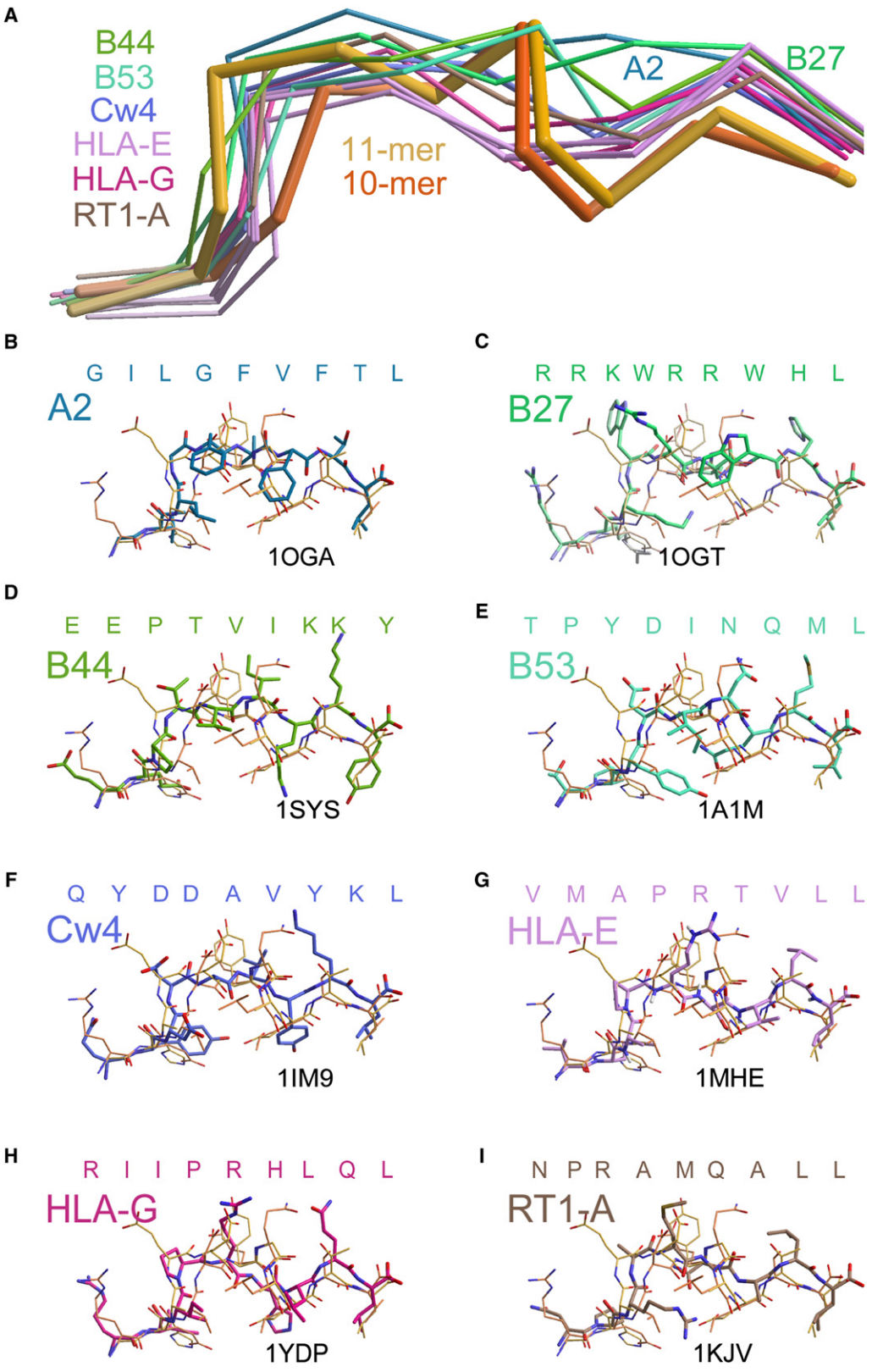

Figure 5. Comparison of Peptides Bound to BF2*2101 with Those Bound to Mammalian Structures

(A) A superposition of the Cα-traces of the 11-mer (yellow) and 10-mer (orange) peptides bound to BF2*2101, peptides bound to the human classical MHC class I molecules HLA-A2 (1OGA, blue), B27 (1OGT, green), B44 (1SYS, green), B53 (1A1M, cyan), and Cw4 (1IM9 and 1QQD, light blue), the

charges on Argα9 and Aspα24 provides a particularly powerful mechanism for charge transfer not previously observed in MHC molecules.

In order to determine how many MHC class I molecules might share these features with BF2*2101, we examined 2114 sequences of classical MHC class I molecules from fish to human, as well as a further 63 nonclassical class I sequences from mouse, rat, and frog (Table S5). Very few classical MHC class I sequences have small residues at either α69(70) or α97(99) [5% Ser, 0.5% Gly and 1.8% Ala for α69(70); 4% Ser, 3% Cys and 0.2% Ala for α97(99)]. Only seven classical sequences (0.3%) have small residues in both positions: BF2*2101 from chicken, two from cottontop tamarin, two from sheep, one from rat, and one from rainbow trout. Moreover, only three nonclassical sequences have small residues in both positions. Thus, an open central cavity appears to be unusual for both classical and nonclassical MHC class I molecules.

Strikingly, these analyses show that Argα9 and Aspα24 have not been found outside of chickens. There are six chicken sequences with Argα9, of which three also have Aspα24, and ten chicken sequences with Hisα9 and Aspα24, but of these, only BF2*2101 has small residues at both α69(70) and α97(99). There are a few classical sequences outside of chickens with basic residues at α9 or acidic residues at α24 (11% His or Lys at α9; 2.7% Glu at α24) but none with both in the same sequence. In rat, there are five nonclassical sequences with both Lysα9 and Gluα24, but none with small residues at α69(70) and α97(99). Thus, the sequence features allowing this precise mode of charge transfer seem to be unique to BF2*2101 among the known classical and nonclassical MHC class I molecules in vertebrates.

The Peptide-Binding Motif Might Explain the Strong Resistance of the B21 Haplotype to Marek's Disease

A large number of studies show that the B21 haplotype confers strong resistance to Marek's disease, which is caused by an oncogenic herpesvirus (Bacon, 1987; Bacon et al., 1987; Briles et al., 1977; Plachy et al., 1992). There are many candidate genes and little recombination in the region identified as being responsible for this resistance (Kaufman et al., 1999a, 1999b; Shiina et al., 2007), so the gene(s) actually responsible are not known. However, several studies propose that this resistance is due to the action of cytotoxic T lymphocytes (CTLs) and/or natural killer (NK) cells (Garcia-Camacho et al., 2003; Markowski-Grimsrud and Schat, 2003; Omar and Schat, 1996; Omar and Schat, 1997), both of which implicate an MHC class I molecule as the target. The distinctive nature of the BF2*2101 molecule is consistent with these proposals.

To illustrate how the distinctive nature of the BF2*2101 could explain the resistance to Marek's disease conferred by the B21 haplotype compared to other well-defined haplotypes, we determined a preliminary peptide motif for this molecule by using assembly of the 10-mer and 11-mer peptides substituted at various positions (Figure S4, Table S6). This is by no means an exhaustive analysis, and so in fact more peptides might have been predicted than are specified by this preliminary motif. However, even at this early stage of analysis, it is clear that many more peptides from representative Marek's disease virus (MDV) genes are predicted to bind the BF2*2101 molecule than the MHC class I molecules from haplotypes such as B4, B12, and B15 that do not confer strong resistance to Marek's disease (Table 2, Table S7). On this basis, it is likely that the promiscuous BF2*2101 molecule would have a greater chance of binding key protective peptide(s) than the fastidious MHC class I molecules from the other haplotypes.

DISCUSSION

Here, we report the first structures of an MHC molecule outside of mammals, the classical class I molecule BF2*2101 from the chicken MHC haplotype B21. This molecule has a novel mode of peptide binding that allows peptides with completely different sequences to be presented to T lymphocytes. Some malleability of adjacent pockets in the peptide binding groove, and resultant interdependence of peptide anchors, has been described for certain mammalian MHC class I molecules. However, BF2*2101 provides an extreme example of such coupled variation, with the conformational freedom and charged nature of the Argα9 side chain allowing very varied combinations of interactions between itself, Aspα24, and peptide residues P_2 and P_{C-2}. One of the examples we describe has an acidic amino acid in the peptide (Glu2 in the 10-mer) interacting with another acidic amino acid in the MHC molecule (Aspα24), supported by the basic amino acid Argα9. Such charge-transfer mechanisms have been described in enzymes such as hemoglobin, cytochrome c peroxidase, carboxypeptidase II (Flocco and Mowbray, 1995), and most recently in the serine-carboxyl-type proteinase Kumamolysin (Comellas-Bigler et al., 2002) but never before in an MHC molecule.

The resulting coupled variation of the peptide residues binding into pocket B and C also explains why the pool sequences and individual peptides for MHC class I molecules from the B21 haplotype led to no clear motif. Interdependent pairs of amino acids at P_2 and P_{C-2} meant these anchor positions could be occupied by amino acids with very different sizes and chemical properties. There are several examples in which pool sequences have not led to consistent motifs or in which single peptides that bind an MHC class I molecule did not fit the motif (Gaddum et al., 1996; Quesnel et al., 1996; Mata et al., 1998;

human nonclassical MHC class I molecules HLA-E (1KPR, 1KTL, 1MHE, and 2ESV, light violet) and HLA-G (1YDP, 2DYP, and 2D31, wine red), and the rat MHC class I molecule RT1-A (1KJV, brown). The 10-mer and 11-mer peptides are highlighted as thicker lines.
(B–I) The structures of selected peptides are depicted as thick stick models (plus sequence in one letter code) superposed with the 10-mer and 11-mer peptides (thin sticks). Carbon atom colors are as above. Cw4, HLA-E, and HLA-G are represented by 1MI9, 1MEH, and 1YDP, respectively.

Table 2. Number of Peptides from MDV Genes Predicted to Bind Class I Molecules from Chicken MHC Haplotypes B4, B12, B15, and B21

Haplotype	gB	pp38	meq	ICP4
B4	0-1	0-1	0	1
B12	8-11	0-3	0	9
B15	0-1	0	2-3	2
B21	15-20	0-3	6-11	14-15

The protein sequences from four MDV genes, considered as likely candidates for protective antigens (Omar and Schat, 1996; Omar and Schat, 1997), were analyzed on the basis of the sequences from the following strains (database entries or references): gB protein: HVT (Q69408), SB1 (Q69406), and RB1B (P18538); pp38 protein: S1 (Q89483), S2 (D28115), and S3 (Q89873); meq protein: RB1B (M89471), GA, HPRS16, C12/130, MR36, and MR48 (Barrow and Venugopal, 1999); and ICP4 protein: GA (Q02362), C12/130, MR36, and MR38 (Barrow and Venugopal, 1999). Peptide motifs and prediction methods were derived from Kaufman et al. (1995); Wallny et al. (2006), and this paper. The motifs were the following: B4: x-(D or E)-x-x-(D or E)-x-x-E; B12: x-x-x-x-(V or I)-x-x-V; B15: (K or R)-R-x-x-x-x-x-Y and (K or R)-R-x-x-x-x-x-x-Y; B21: x-(H, K or R)-x-x-x-x-x-x-(E or D)-x-(A, V, L, I, F or W), x-(H, K or R)-x-x-x-x-x-(E or D)-x-(A V, L, I, F or W), x-(E or D)-x-x-x-x-x-L-x-(A, V, L, I, F or W) and x-(E or D)-x-x-x-x-x-x-L-x-(A, V, L, I, F or W). The predominant lengths of peptide found in single and pool sequences were octamers for B4 and B12, octamers and nonamers for B15, and 10-mers and 11-mers for B21. Although longer peptides (nonamers and longer for B4 and B12, 10-mers and longer for B15, and 12-mers and longer for B21) and shorter peptides (nonamers for B21) are also found and can also assemble, they are rare. So for comparison's sake, only the predominant length was used for the motifs. There are also a number of hydrophobic residues found at the C terminus of peptides for B4, B12, and B15, but again, they are rare, so for comparison's sake, they were not used in the motif.

Apostolopoulos and Lazoura, 2004). Some of these cases might also be due to binding mechanisms that involve coupled variation of the anchor residues. Our data also suggest caution in the development of peptide prediction algorithms and peptide modeling projects that might not take account of such promiscuity, thus failing to predict functionally important peptides.

The chicken MHC class I molecule BF2*2101 is encoded by the B21 haplotype, which is known for having one of the strongest associations with resistance to an infectious pathogen, the economically important herpesvirus that causes Marek's disease (Briles et al., 1977; Bacon, 1987; Plachy et al., 1992). It has not been possible to assign the MHC-determined resistance to Marek's disease to a particular gene because of the rarity of recombination within the chicken MHC (BF/BL region). However, a number of studies have suggested that the MHC-determined resistance to Marek's disease is due at least in part to the action of CTLs and NK cells (Garcia-Camacho et al., 2003; Markowski-Grimsrud and Schat, 2003; Omar and Schat, 1996; Omar and Schat, 1997), both of which implicate an MHC class I molecule as a target. The data presented in this paper suggest that BF2*2101 is distinctive and provide support for the notion that it might be responsible for the strong resistance conferred by this haplotype, as illustrated by epitope predictions made on the basis of a preliminary peptide motif. Moreover, given that the B21 haplotype is very common in chickens (Simonsen et al., 1982), these data might be useful for developing vaccines, not only to MDV, but to other pathogens, such as avian influenza.

EXPERIMENTAL PROCEDURES

Isolation of MHC Class I Molecules and Analysis of Peptides

Methods were identical to those of Wallny et al. (2006), including affinity chromatography of class I molecules, peptide isolation and chromatography, Edman degradation of peptide pools and individual peptides, and mass spectrometry (MS/MS) of individual peptides. For spleen preparations, the capsules were removed, the spleens were ground up in an equal volume of phosphate-buffered saline with 10 mM $MgCl_2$, 0.4 mM 4-(2-aminoethyl) benzenesulfonyl fluoride hydrochloride (AEBSF), and 0.4 mM iodoacetamide on ice with a loose glass tissue homogenizer, and NP-40 detergent was added to 2.5% final concentration. The lysate was incubated on ice for 30 min and centrifuged twice at 4,000 rpm in a Sorvall GSA rotor, twice at 13,500 rpm, and one to three times at 20,000 rpm in a Sorval SLA 600TC rotor, each spin for 30 min at 4°C.

Assembly of Denatured BF2*2101 and β_2m with Peptides and Peptide Libraries

Overall, methods followed those of Dunbar et al. (1998). In brief, complementary DNA (cDNA) was used for amplification of a β_2m sequence encoding the mature protein without a signal sequence but beginning with a start codon. A cDNA clone of BF2*2101 was used as a source for amplification of the α1-α2-α3 domains (residues 1–270 of the mature protein), which was cloned into pBluescript, engineered to have a start codon at the beginning and a biotinylation sequence followed by a His tag at the end. Both sequences were cloned into pET22b(+), and proteins were expressed as inclusion bodies in BL21 (λDE3) pLysS Rosetta cells. Inclusion bodies were isolated and dissolved in solutions containing urea. Peptides were synthesized with fluorenyl-methoxycarbonyl (fMOC) chemistry. The denatured proteins were renatured in the presence of peptides or peptide libraries, and monomers were separated from aggregates, heavy chains, β_2m, peptides, and smaller molecules by fast protein liquid chromatography (FPLC) size exclusion chromatography with a HiLoad 26/60 Superdex 200 column (Pharmacia).

Sequence Comparisons

MHC class I sequences were sourced as follows: human (IMGT/HLA database; www.ebi.ac.uk/imgt/hla), nonhuman primates and monkeys, cattle, sheep, swine, rat, and bony fish (IPD-MHC databases; www.ebi.ac.uk/ipd), mouse (Watts et al., 1989), bird (Wallny et al., 2006; Livant et al., 2004; Lima-Rosa et al., 2004; Hunt and Fulton, 1998; Shiina et al., 1999; Moon et al., 2005), frog (Flajnik et al., 1993; Flajnik et al., 1999) and shark (Okamura et al., 1997).

Crystallization

Renatured proteins were concentrated to 10 mg/ml in 50mM NaCl, 10mM Tris (pH 8.0) and crystallized by the sitting-drop vapor-diffusion method. The crystallizations were set up as nanoliter scale drops (100 nL of protein plus 100 nL of reservoir solution) with a Cartesian Technologies Microsys MIC4000 (Genomic Technologies) (Walter et al., 2003).

Crystals grew at room temperature in 0.1 M HEPES (pH 7.0), 100 mM $MgCl_2$, and 27% polyethylene glycol 3350. The BF2*2101-11-mer

crystals were long thin needles of dimensions 300 × 30 × 30 μm^3, whereas those of BF2*2101-10-mer were larger and multiple, with the lengths of about 100 μm in all three dimensions. Both crystal types were soaked briefly in per-fluoropolyether oil (PFPE) before being flash cooled and maintained at 100°K in a cryostream. Data collection for the BF2*2101-11-mer was straightforward; however, the BF2*2101-10-mer required careful selection of suitable portions of crystal and orientation ranges to minimize problems with multiple overlapping lattices.

Diffraction data were recorded at station BM14 of the European Synchrotron Radiation Facility (ESRF [Grenoble, France]) with a MARCCD m225 CCD detector. Diffraction datasets were autoindexed with Denzo and scaled together with Scalepack (Otwinowski and Minor, 1997) (http://www.hkl-xray.com) (Table 1). The asymmetric unit of BF2*2101-11-mer contained a single molecule and 47% solvent, whereas that of BF2*2101-10-mer had two molecules with 61% solvent.

Structure Determination and Refinement

The structure of BF2*2101-11-mer was determined by molecular replacement with a human HLA-B27 structure (PDB-entry 1OGT with peptide coordinates removed) on the webmail interface CaspR (http://igs-server.cnrs-mrs.fr/Caspr/index.cgi/). The α3 domain required manual reorientation into initial low-quality $2F_o$-F_c electron density. After further domain-wise rigid-body refinement, the model was rebuilt (with BF2*2101 sequence) into much improved $2F_o$-F_c electron density and refined by simulated annealing with CNS (Brunger et al., 1998) (http://cns.csb.yale.edu/). After model building by ARP-wARP (Morris et al., 2003), the peptide was added. Positional refinement and individual B factor refinement with bulk solvent scaling and overall anisotropic B- actor scaling were applied, interspersed with manual rebuilding with O (http://www.bioxray.dk/~mok/o-files.html). Water molecules were added with ARP-wARP (based on F_o-F_c peaks of at least 2.5 σ), and refinement was completed with translation, libration, and screw rotation (TLS) in the REFMAC CCP4 program suite (Collaborative Computational Project, 1994; Murshudov et al., 1997; Winn et al., 2001) (http://www.ccp4.ac.uk). The final structure had good stereochemistry (Table 1), as assessed by the program PROCHECK (Laskowski et al., 1993), with R_{work} 23.0% and R_{free} 28.6%, comprising residues 1–274 of the heavy chain, 1–99 of the β_2m, and 190 water molecules.

The structure of BF2*2101-10-mer was determined by molecular replacement with the BF2*2101-11-mer structure as the search model in MOLREP (Vagin and Teplyakov, 1997). After initial rigid-body refinement and some cycles of restrained refinement with REFMAC, further modeling was guided by F_o-F_c and $2F_o$-F_c electron density maps calculated with REFMAC and by simulated annealing and composite OMIT maps calculated with CNS. Subsequent refinement in REFMAC was as described above but with noncrystallographic symmetry (NCS) restraints applied to the two copies of BF2*2101-10-mer in the asymmetric unit. The final refined structure had good stereochemistry (Table 1), as assessed by the program PROCHECK (Laskowski et al., 1993), with R_{work} 23.4% and R_{free} 29.5%, comprising residues 1–271 of the heavy chain and residues 1–99 in β_2m for both copies, and 129 water molecules.

Structural Analysis and Modeling

Overall and domain-wise superpositions of pairs of structures were calculated with the program SHP (Stuart et al., 1979). The structures of the two copies of BF2*2101-10-mer in the crystallographic asymmetric unit were essentially identical, as was the BF2*2101-11-mer (Table 1). Superpositions of peptides from mammalian structures onto the peptides bound to BF2*2101 were done with the program IMPOSE (R. Esnouf, personal communication), with a "core set" of framework residues (5–13, 21–26, 31–37, 43–47, 54–86, 91–101, 107–123, and 136–175 numbered as in BF2*2101).

Structural figures were prepared with Bobscript (Esnouf, 1999) and Raster3D (Merritt and Murphy, 1994) (http://trantor.bioc.columbia.edu/grasp/). Cavity volumes and maps were calculated with the program VOLUMES (R. Esnouf, personal communication) with a 1.4 Å probe radius so that the accessibility of the surface of the molecules to the solvent as well as inside the molecule could be assessed.

Supplemental Data

Four figures and seven tables are available at http://www.immunity.com/cgi/content/full/27/6/885/DC1/.

ACKNOWLEDGMENTS

We thank Division of Structural Biology (STRUBI) members for assistance and helpful discussions, K. Harlos, R. Esnouf, and staff of the European Synchrotron Radiation Facility (ESRF) and European Molecular Biology Laboratory (EMBL) in Grenoble for assistance with X-ray data collection, Susan Lea and Gillian Griffiths for critical reading and suggestions, and the United Kingdom Medical Research Council (E.Y.J.), Biotechnology and Biological Sciences Research Council (BBSRC) (J.K.) and European Union (PeptidEx consortium; grant code QLK2-CT-2002-000838; J.K.) for funding. We acknowledge use of crystallization facilities provided by the Medical Research Council-funded Oxford Protein Production Facility and the EU Integrated Programme (Structural Proteomics in Europe [SPINE], Grant code QLRT-2001-00988). E.Y.J. is a Cancer Research UK Principal Research Fellow.

Received: February 16, 2007
Revised: October 10, 2007
Accepted: November 2, 2007
Published online: December 13, 2007

REFERENCES

Apostolopoulos, V., and Lazoura, E. (2004). Noncanonical peptides in complex with MHC class I. Expert Rev. Vaccines *3*, 151–162.

Bacon, L. (1987). Influence of the major histocompatibility complex on disease resistance and productivity. Poult. Sci. *66*, 802–811.

Bacon, L., Ismail, N., and Motta, J. (1987). Allograft and antibody responses of 15I5-B congenic chickens. Prog. Clin. Biol. Res. *238*, 219–233.

Barrow, A., and Venugopal, K. (1999). Molecular characterisation of very virulent European MDV isolates. Acta Virol. *43*, 90–93.

Briles, W., Stone, H., and Cole, R. (1977). Marek's disease: Effects of *B* histocompatibility alloalleles in resistant and susceptible chicken lines. Science *195*, 193–196.

Brunger, A., Adams, P., Clore, G., DeLano, W., Gros, P., Grosse-Kunstleve, R., Jiang, J., Kuszewski, J., Nilges, M., Pannu, N., et al. (1998). Crystallography & NMR system: A new software suite for macromolecular structure determination. Acta Crystallogr. D Biol. Crystallogr. *54*, 905–921.

Collaborative Computational Project (1994). The CCP4 suite: Programs for protein crystallography. Acta Crystallogr. D Biol. Crystallogr. *50*, 760–763.

Comellas-Bigler, M., Fuentes-Prior, P., Maskos, K., Huber, R., Oyama, H., Uchida, K., Dunn, B., Oda, K., and Bode, W. (2002). The 1.4 a crystal structure of kumamolysin: A thermostable serine-carboxyl-type proteinase. Structure *10*, 865–876.

Dunbar, P., Ogg, G., Chen, J., Rust, N., van der Bruggen, P., and Cerundolo, V. (1998). Direct isolation, phenotyping and cloning of low-frequency antigen-specific cytotoxic T lymphocytes from peripheral blood. Curr. Biol. *8*, 413–416.

Esnouf, R. (1999). Further additions to MolScript version 1.4, including reading and contouring of electron-density maps. Acta Crystallogr. D Biol. Crystallogr. *55*, 938–940.

Flajnik, M., and Kasahara, M. (2001). Comparative genomics of the MHC: Glimpses into the evolution of the adaptive immune system. Immunity *15*, 351–362.

Flajnik, M., Kasahara, M., Shum, B., Salter-Cid, L., Taylor, E., and Du Pasquier, L. (1993). A novel type of class I gene organization in vertebrates: A large family of non-MHC-linked class I genes is expressed at the RNA level in the amphibian Xenopus. EMBO J. *12*, 4385–4396.

Flajnik, M., Ohta, Y., Greenberg, A., Salter-Cid, L., Carrizosa, A., Du Pasquier, L., and Kasahara, M. (1999). Two ancient allelic lineages at the single classical class I locus in the Xenopus MHC. J. Immunol. *163*, 3826–3833.

Flocco, M., and Mowbray, S. (1995). Strange bedfellows: interactions between acidic side-chains in proteins. J. Mol. Biol. *254*, 96–105.

Fremont, D., Matsumura, M., Stura, E., Peterson, P., and Wilson, I. (1992). Crystal structures of two viral peptides in complex with murine MHC class I H-2Kb. Science *257*, 919–927.

Fremont, D., Stura, E., Matsumura, M., Peterson, P., and Wilson, I. (1995). Crystal structure of an H-2Kb-ovalbumin peptide complex reveals the interplay of primary and secondary anchor positions in the major histocompatibility complex binding groove. Proc. Natl. Acad. Sci. USA *92*, 2479–2483.

Gaddum, R., Willis, A., and Ellis, S. (1996). Peptide motifs from three cattle MHC (BoLA) class I antigens. Immunogenetics *43*, 238–239.

Gao, G., Tormo, J., Gerth, U., Wyer, J., McMichael, A., Stuart, D., Bell, J., Jones, E., and Jakobsen, B. (1997). Crystal structure of the complex between human CD8alpha(alpha) and HLA-A2. Nature *387*, 630–634.

Garcia-Camacho, L., Schat, K., Brooks, R., and Bounous, D.I. (2003). Early cell-mediated immune responses to Marek's disease virus in two chicken lines with defined major histocompatibility complex antigens. Vet. Immunol. Immunopathol. *95*, 145–153.

Guillemot, F., Billault, A., Pourquie, O., Behar, G., Chausse, A., Zoorob, R., Kreibich, G., and Auffray, C. (1988). A molecular map of the chicken major histocompatibility complex: The class II beta genes are closely linked to the class I genes and the nucleolar organizer. EMBO J. *7*, 2775–2785.

Hansen, M., Van Zandt, J., and Law, G. (1967). Differences in susceptibility to Marek's disease in chickens carrying two different B locus blood group alleles. Poult. Sci. *46*, 1268.

Hulsmeyer, M., Fiorillo, M., Bettosini, F., Sorrentino, R., Saenger, W., Ziegler, A., and Uchanska-Ziegler, B. (2004). Dual HLA-B27 subtype-dependent conformation of a self-peptide. J. Exp. Med. *199*, 271–281.

Hunt, H., and Fulton, J. (1998). Analysis of polymorphisms in the major expressed class I locus (B-FIV) of the chicken. Immunogenetics *47*, 456–467.

Hutt, F., and Cole, R. (1947). Genetic control of lymphomatosis in the fowl. Science *106*, 379–384.

Kaufman, J. (1999). Co-evolving genes in MHC haplotypes: The "rule" for nonmammalian vertebrates? Immunogenetics *50*, 228–236.

Kaufman, J., Andersen, R., Avila, D., Engberg, J., Lambris, J., Salomonsen, J., Welinder, K., and Skjødt, K. (1992). Different features of the MHC class I heterodimer have evolved at different rates: Chicken B-F and β_2-microglobulin sequences reveal invariant surface residues. J. Immunol. *148*, 1532–1546.

Kaufman, J., Salomonsen, J., and Flajnik, M. (1994). Evolutionary conservation of MHC class I and class II molecules–different yet the same. Semin. Immunol. *6*, 411–424.

Kaufman, J., Volk, H., and Wallny, H. (1995). A "minimal essential Mhc" and an "unrecognized Mhc": Two extremes in selection for polymorphism. Immunol. Rev. *143*, 63–88.

Kaufman, J., Milne, S., Gobel, T., Walker, B., Jacob, J., Auffray, C., Zoorob, R., and Beck, S. (1999a). The chicken B locus is a minimal essential major histocompatibility complex. Nature *401*, 923–925.

Kaufman, J., Jacob, J., Shaw, I., Walker, B., Milne, S., Beck, S., and Salomonsen, J. (1999b). Gene organisation determines evolution of function in the chicken MHC. Immunol. Rev. *167*, 101–117.

Kelley, J., Walter, L., and Trowsdale, J. (2005). Comparative genomics of major histocompatibility complexes. Immunogenetics *56*, 683–695.

Kern, P., Teng, M., Smolyar, A., Liu, J., Liu, J., Hussey, R., Spoerl, R., Chang, H., Reinherz, E., and Wang, J. (1998). Structural basis of CD8 coreceptor function revealed by crystallographic analysis of a murine CD8alphaalpha ectodomain fragment in complex with H-2Kb. Immunity *9*, 519–530.

Khan, A., Baker, B., Ghosh, P., Biddison, W., and Wiley, D.C. (2000). The structure and stability of an HLA-A*0201/octameric tax peptide complex with an empty conserved peptide-N-terminal binding site. J. Immunol. *164*, 6398–6405.

Kjer-Nielsen, L., Clements, C., Purcell, A., Brooks, A., Whisstock, J., Burrows, S., McCluskey, J., and Rossjohn, J. (2003). A structural basis for the selection of dominant alpha beta T cell receptors in antiviral immunity. Immunity *18*, 53–64.

Laskowski, R., MacArthur, M., Moss, D., and Thornton, J. (1993). PROCHECK: A program to check the stereochemical quality of protein structures. J. Appl. Cryst. *26*, 283–291.

Li, H., Robertson, A., and Jensen, J. (2005). Very fast empirical prediction and interpretation of protein pKa values. Proteins *61*, 704–721.

Lima-Rosa, C., Canal, C., Streck, A., Freitas, L., Delgado-Canedo, A., Bonatto, S., and Salzano, F. (2004). B-F DNA sequence variability in Brazilian (blue-egg Caipira) chickens. Anim. Genet. *35*, 278–284.

Livant, E., Brigati, J., and Ewald, S. (2004). Diversity and locus specificity of chicken MHC B class I sequences. Anim. Genet. *35*, 18–27.

Madden, D. (1995). The three-dimensional structure of peptide-MHC complexes. Annu. Rev. Immunol. *13*, 587–622.

Madden, D., Garboczi, D., and Wiley, D. (1993). The antigenic identity of peptide-MHC complexes: A comparison of the conformations of five viral peptides presented by HLA-A2. Cell *75*, 693–708.

Markowski-Grimsrud, C., and Schat, K. (2003). Infection with chicken anaemia virus impairs the generation of pathogen-specific cytotoxic T lymphocytes. Immunology *109*, 283–294.

Mata, M., Travers, P., Liu, Q., Frankel, F., and Paterson, Y. (1998). The MHC class I-restricted immune response to HIV-gag in BALB/c mice selects a single epitope that does not have a predictable MHC-binding motif. J. Immunol. *161*, 2985–2993.

Matsumura, M., Fremont, D., Peterson, P., and Wilson, I. (1992). Emerging principles for the recognition of peptide antigens by MHC class I molecules. Science *257*, 27–34.

Merritt, E., and Murphy, M. (1994). Raster3D Version 2.0. A program for photorealistic molecular graphics. Acta Crystallogr. D Biol. Crystallogr. *50*, 869–873.

Moon, D., Veniamin, S., Parks-Dely, J., and Magor, K. (2005). The MHC of the duck (Anas platyrhynchos) contains five differentially expressed class I genes. J. Immunol. *175*, 6702–6712.

Morris, R., Perrakis, A., and Lamzin, V. (2003). ARP/wARP and automatic interpretation of protein electron density maps. Methods Enzymol. *374*, 229–244.

Murshudov, G., Vagin, A., and Dodson, E. (1997). Refinement of macromolecular structures by the maximum-likelihood method. Acta Crystallogr. D Biol. Crystallogr. *53*, 240–255.

Okamura, K., Ototake, M., Nakanishi, T., Kurosawa, Y., and Hashimoto, K. (1997). The most primitive vertebrates with jaws possess highly polymorphic MHC class I genes comparable to those of humans. Immunity *7*, 777–790.

Omar, A., and Schat, K. (1996). Syngeneic Marek's disease virus (MDV)-specific cell-mediated immune responses against immediate early, late and unique MHC proteins. Virology *222*, 87–99.

Omar, A., and Schat, K. (1997). Characterization of Marek's disease herpesvirus-specific cytotoxic T lymphocytes in chickens inoculated

with a non-oncogenic vaccine strain of MDV. Immunology *90*, 579–585.

Otwinowski, Z., and Minor, W. (1997). Processing of X-ray diffraction data collected in oscillation mode. Methods Enzymol. *276*, 307–326.

Plachy, J., Pink, J., and Hala, K. (1992). Biology of the chicken MHC (B complex). Crit. Rev. Immunol. *12*, 47–79.

Probst-Kepper, M., Hecht, H., Herrmann, H., Janke, V., Ocklenburg, F., Klempnauer, J., van den Eynde, B., and Weiss, S. (2004). Conformational restraints and flexibility of 14-meric peptides in complex with HLA-B*3501. J. Immunol. *173*, 5610–5616.

Quesnel, A., Hsu, S., Delmas, A., Steward, M., Trudelle, Y., and Abastado, J. (1996). Efficient binding to the MHC class I K(d) molecule of synthetic peptides in which the anchoring position 2 does not fit the consensus motif. FEBS Lett. *387*, 42–46.

Rammensee, H. (1995). Chemistry of peptides associated with MHC class I and class II molecules. Curr. Opin. Immunol. *7*, 85–96.

Rammensee, H., Friede, T., and Stevanoviic, S. (1995). MHC ligands and peptide motifs: First listing. Immunogenetics *41*, 178–228.

Reid, S., McAdam, S., Smith, K., Klenerman, P., O'Callaghan, C., Harlos, K., Jakobsen, B., McMichael, A., Bell, J., Stuart, D., and Jones, E. (1996). Antagonist HIV-1 Gag peptides induce structural changes in HLA B8. J. Exp. Med. *184*, 2279–2286.

Rudolph, M., Speir, J., Brunmark, A., Mattsson, N., Jackson, M., Peterson, P., Teyton, L., and Wilson, I. (2001). The crystal structures of K(bm1) and K(bm8) reveal that subtle changes in the peptide environment impact thermostability and alloreactivity. Immunity *14*, 231–242.

Saper, M., Bjorkman, P., and Wiley, D. (1991). Refined structure of the human histocompatibility antigen HLA-A2 at 2.6 A resolution. J. Mol. Biol. *219*, 277–319.

Shiina, T., Oka, A., Imanishi, T., Hanzawa, K., Gojobori, T., Watanabe, S., and Inoko, H. (1999). Multiple class I loci expressed by the quail Mhc. Immunogenetics *49*, 456–460.

Shiina, T., Briles, W., Goto, R., Hosomichi, K., Yanaqiya, K., Shimizu, S., Inoko, H., and Miller, M. (2007). Extended gene map reveals tripartite motif, C-type lectin and Ig superfamily type genes within a subregion of the chicken MHC-B affecting infectious disease. J. Immunol. *178*, 7162–7172.

Simonsen, M., Crone, M., Koch, C., and Hala, K. (1982). The MHC haplotypes of the chicken. Immunogenetics *16*, 513–532.

Smith, K., Reid, S., Harlos, K., McMichael, A., Stuart, D., Bell, J., and Jones, E. (1996). Bound water structure and polymorphic amino acids act together to allow the binding of different peptides to MHC class I HLA-B53. Immunity *4*, 215–228.

Speir, J., Stevens, J., Joly, E., Butcher, G., and Wilson, I. (2001). Two different, highly exposed, bulged structures for an unusually long peptide bound to rat MHC class I RT1-Aa. Immunity *14*, 81–92.

Stern, L., and Wiley, D. (1994). Antigenic peptide binding by class I and class II histocompatibility proteins. Structure *2*, 245–251.

Stuart, D., Levine, M., Muirhead, H., and Stammers, D. (1979). Crystal structure of cat muscle pyruvate kinase at a resolution of 2.6 A. J. Mol. Biol. *134*, 109–142.

Tynan, F., Burrows, S., Buckle, A., Clements, C., Borg, N., Miles, J., Beddoe, T., Whisstock, J., Wilce, M., Silins, S., et al. (2005). T cell receptor recognition of a 'super-bulged' major histocompatibility complex class I-bound peptide. Nat. Immunol. *6*, 1114–1122.

Vagin, A., and Teplyakov, A. (1997). MOLREP: An automated program for molecular replacement. J. Appl. Cryst. *30*, 1022–1025.

Wallny, H., Avila, D., Hunt, L., Powell, T., Riegert, P., Salomonsen, J., Skjodt, K., Vainio, O., Vilbois, F., Wiles, M., and Kaufman, J. (2006). Peptide motifs of the single dominantly expressed class I molecule explain the striking MHC-determined response to Rous sarcoma virus in chickens. Proc. Natl. Acad. Sci. USA *103*, 1434–1439.

Walter, T., Diprose, J., Brown, J., Pickford, M., Owens, R., Stuart, D., and Harlos, K. (2003). A procedure for setting up high-throughput nanolitre crystallization experiments. I. Protocol design and validation. J. Appl. Cryst. *36*, 308–314.

Watts, S., Wheeler, C., Morse, R., and Goodenow, R. (1989). Amino acid comparison of the class I antigens of mouse major histocompatibility complex. Immunogenetics *30*, 390–392.

Wilson, I., and Fremont, D. (1993). Structural analysis of MHC class I molecules with bound peptide antigens. Semin. Immunol. *5*, 75–80.

Winn, M., Isupov, M., and Murshudov, G. (2001). Use of TLS parameters to model anisotropic displacements in macromolecular refinement. Acta Crystallogr. D Biol. Crystallogr. *57*, 122–133.

Accession Numbers

Coordinates and structure factors have been deposited in the Protein Data Bank under accession codes 3BEV (BF2*2101-11-mer) and 3BEW (BF2*2101-10-mer).